Resonant Second-Harmonic Generation as a Probe of Quantum Geometry

Pankaj Bhalla,[1,2,3,*,‖] Kamal Das,[4,†,‖] Dimitrie Culcer,[3,5,‡] and Amit Agarwal[4,§]
[1]Department of Physics, School of Engineering and Sciences, SRM University AP, Amaravati, 522240, India
[2]Beijing Computational Science Research Center, Beijing 100193, China
[3]ARC Centre of Excellence in Future Low-Energy Electronics Technologies, The University of New South Wales, Sydney 2052, Australia
[4]Department of Physics, Indian Institute of Technology Kanpur, Kanpur-208016, India
[5]School of Physics, The University of New South Wales, Sydney 2052, Australia

(Received 16 August 2021; revised 6 March 2022; accepted 14 October 2022; published 23 November 2022)

Nonlinear responses are actively studied as probes of topology and band geometric properties of solids. Here, we show that second harmonic generation serves as a probe of the Berry curvature, quantum metric, and quantum geometric connection. We generalize the theory of second harmonic generation to include Fermi surface effects in metallic systems, and finite scattering timescale. In doped materials the Fermi surface and Fermi sea cause all second harmonic terms to exhibit resonances, and we identify two novel contributions to the second harmonic signal: a double resonance due to the Fermi surface and a higher-order pole due to the Fermi sea. We discuss experimental observation in the monolayer of time reversal symmetric Weyl semimetal WTe_2 and the parity-time reversal symmetric topological antiferromagnet CuMnAs.

DOI: 10.1103/PhysRevLett.129.227401

The quantum geometric properties of the electron wave function give rise to a multitude of electronic transport effects [1–13]. In optical phenomena the Berry phase plays a fundamental role in photogalvanic responses [14,15], circular photogalvanic effect [16,17], and in other nonlinear optical responses [18–22]. The Berry curvature dipole and the quantum metric are likewise key in determining nonlinear optical responses [20,23–35]. Fundamental interest in the band geometric properties of quantum materials has been responsible for the recent resurgence of nonlinear phenomena, driving basic discoveries. Prominent examples include nonreciprocal currents [36–40], Hall effects in time-reversal invariant systems [41–46], and using nonlinear susceptibilities to probe details of the crystallographic orientation, band structure, and grain boundaries [47,48]. However, the interplay between band geometric quantities that gives rise to the photogalvanic effect, second harmonic (SH) response [25,49–56] as well as higher harmonic generation [57–60], is not fully understood [34,61–80]. In fact, the theory of SH generation itself has two key shortcomings: (i) missing terms which arise in the presence of a finite Fermi surface in metallic or semimetallic systems, (ii) missing terms which arise in the presence of disorder. Additionally, the theory of SH generation in parity-time reversal symmetric systems is relatively less explored.

Motivated by these, we generalize the theory of SH generation [24,25] to include the effect of finite Fermi surface in metallic systems and the effect of disorder. Our central result is encapsulated in Figs. 1 and 2, showing the SH response in the monolayer of the time reversal symmetric Weyl semimetal WTe_2 and the parity-time reversal symmetric topological antiferromagnet CuMnAs,

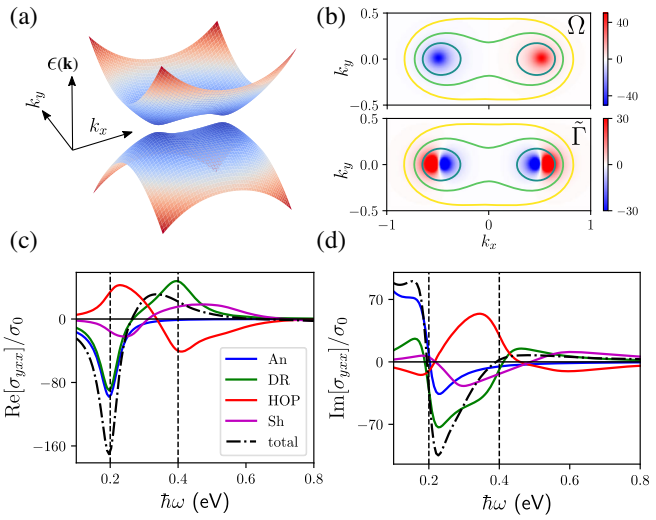

FIG. 1. (a) Band dispersion for monolayer WTe_2 [from Eq. (6)]. We have set the tilt $A = 0$, gap parameters $\delta = -0.25$, $D = 0.1$ in eV and the other parameters to be $B = 1.0$ eV Å^{-2}, $v_y = 1$ eV Å^{-1}. (b) The momentum space distribution of Ω^{xy}_{cv} (top) and the symplectic connection $\tilde{\Gamma}^{yxx}_{cv}$ (bottom), where cv denotes conduction and valence band. Frequency dependence of the different contributions to the (c) real and (d) imaginary parts of the conductivity σ_{yxx}. The conductivities are expressed in units of $\sigma_0 = 10^{-5}$ nA m/V^2. We have set $\mu = 0.2$ eV, $\tau = 1$ ps and temperature $T = 12$ K.

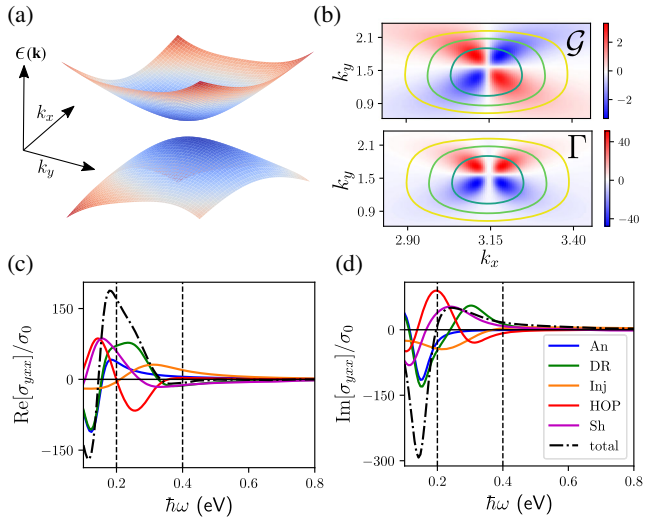

FIG. 2. (a) Band dispersion for $\mathcal{PT}$-symmetric CuMnAs [Eq. (7)]. Here, we set the hopping $t = 0.08$ eV and $\tilde{t} = 1$ eV. The other parameters are $\alpha_R = 0.8$, $\alpha_D = 0$, and $\boldsymbol{h}_{AF} = (0, 0, 0.85)$ eV. (b) The momentum space distribution of $\mathcal{G}^{xy}_{cv}$ (top) and the metric connection Γ^{yxx}_{cv} (bottom). Frequency dependence of the different contributions in the (c) real and (d) imaginary parts of the SH conductivity σ_{yxx}. The conductivities are expressed in units of $\sigma_0 = 10^{-5}$ nA m/V^2, while $\mu = 0.2$ eV, $\tau = 1$ ps, and temperature $T = 12$ K.

represented here by the Hall signal. Remarkably, the SH response exhibits two extrema: one in the vicinity of the chemical potential μ and one in the vicinity of 2μ. These result from the interplay of five distinct contributions related to the quantum geometric properties of the wave function (see Table I), which are *all* resonant. The strongest contributions to the peaks stem from Fermi surface terms we denote as anomalous and doubly resonant, as well as a higher-order pole term from the Fermi sea. The latter two, whose existence was previously unknown, are always opposite in sign, in a striking analogy to the anomalous Hall effect in magnetic materials [81].

These findings can be understood in terms of a systematic quantum geometrical classification, which we achieve by formulating the theory of SH generation within the quantum kinetic framework. We show that the SH current is primarily determined by four geometrical quantities, the Berry curvature (Ω), the quantum metric ($\mathcal{G}$), the metric connection (Γ), and the symplectic connection ($\tilde{\Gamma}$). The former two are the real and imaginary parts of the quantum geometric tensor ($\mathcal{Q} = \mathcal{G} - i\Omega/2$) while the latter two define the quantum geometric connection ($\mathcal{C} = \Gamma - i\tilde{\Gamma}$), respectively [17,19]. By an appropriate choice of material, the extrema in the SH response probe either the Berry curvature or the elusive quantum metric [83]. In time reversal ($\mathcal{T}$) symmetric systems, such as monolayer WTe_2, the shift contribution depends only on $\tilde{\Gamma}$, while the other four contributions rely only on Ω. In contrast, in parity-time reversal symmetric ($\mathcal{PT}$) systems, such as CuMnAs, the SH shift contribution is determined by Γ, while all other geometric contributions are determined by $\mathcal{G}$. We show that the SH injection current vanishes in $\mathcal{T}$-symmetric systems, while all the current components are finite in $\mathcal{PT}$-symmetric systems. Although we focus on topological materials, the conclusions hold generally for insulators and metals.

The quantum kinetic equation for the density matrix $\rho(\boldsymbol{k}, t)$ in the crystal momentum representation is

$$\frac{\partial \rho(\boldsymbol{k},t)}{\partial t} + \frac{i}{\hbar}[\mathcal{H}(\boldsymbol{k},t), \rho(\boldsymbol{k},t)] + \frac{1}{\tau}[\rho(\boldsymbol{k},t) - \rho^{(0)}(\boldsymbol{k},t)] = 0. \tag{1}$$

TABLE I. Different terms leading to second harmonic (2ω) current in response to a harmonic electromagnetic field [see Eq. (5)]. The SH conductivity is given by the relation, $j^{(2)}_a(2\omega) = \sum_{bc} \sigma_{abc}(2\omega) E_b(\omega) E_c(\omega)$ and the SH conductivities are defined to be symmetric under the exchange of the last two indices. This is achieved via the relation, $\sigma_{abc} = \sigma_{acb} = -1/(2\pi)^d (e^3/\hbar^2) \int d^d k [\mathcal{I}_{abc} + \mathcal{I}_{acb}]/2$. We define the quantum metric as $\mathcal{G}^{cb}_{mp} = \{\mathcal{R}^c_{pm}, \mathcal{R}^b_{mp}\}/2$, the Berry curvature as $\Omega^{cb}_{mp} = i[\mathcal{R}^c_{pm}, \mathcal{R}^b_{mp}]$ [21], and the metric connection (Γ) and symplectic connection ($\tilde{\Gamma}$) terms as $\mathcal{R}^a_{pm}\mathcal{D}^b_{mp}\mathcal{R}^c_{mp} = \Gamma^{abc}_{mp} - i\tilde{\Gamma}^{abc}_{mp}$, where $\mathcal{D}^b_{mp} = \partial_b - i(\mathcal{R}^b_{mm} - \mathcal{R}^b_{pp})$. Corresponding to each SH current component, there is also a photogalvanic (dc) counterpart, which can be obtained via the substitution $g^{2\omega}_{mp} \to g^{\omega=0}_{mp}$ and $g^{2\omega}_0 \to g^{\omega=0}_0$ (see Table S1 in SM [82]).

Current	Integrand	Geometrical quantity	$\mathcal{T}$	$\mathcal{PT}$	Physical origin
Drude	$\mathcal{I}^{\mathrm{D}}_{abc} = g^{\omega}_0 g^{2\omega}_0 \sum_m (1/\hbar)(\partial\varepsilon_m/\partial k_a)(\partial^2 f^{(0)}_m/\partial k_b \partial k_c)$	None	0	$\neq 0$	Nonequilibrium distribution function
Injection	$\mathcal{I}^{\mathrm{Inj}}_{abc} = -g^{2\omega}_0 \sum_{pm} g^{\omega}_{mp}(\partial\omega_{mp}/\partial k_a)(\mathcal{G}^{bc}_{mp} - i\Omega^{bc}_{mp}/2)F_{mp}$	Ω, $\mathcal{G}$	Ω	$\mathcal{G}$	Velocity injection along current
Shift	$\mathcal{I}^{\mathrm{Sh}}_{abc} = \sum_{pm} \omega_{mp} g^{2\omega}_{mp} g^{\omega}_{mp}(\Gamma^{abc}_{mp} - i\tilde{\Gamma}^{abc}_{mp})F_{mp}$	$\tilde{\Gamma}$, Γ	$\tilde{\Gamma}$	Γ	Shift of the wave packet
Anomalous	$\mathcal{I}^{\mathrm{An}}_{abc} = g^{\omega}_0 \sum_{pm} \omega_{mp} g^{2\omega}_{mp}(\mathcal{G}^{ab}_{mp} - i\Omega^{ab}_{mp}/2)(\partial F_{mp}/\partial k_c)$	Ω, $\mathcal{G}$	Ω	$\mathcal{G}$	Fermi surface
DR	$\mathcal{I}^{\mathrm{DR}}_{abc} = \sum_{pm} \omega_{mp} g^{\omega}_{mp} g^{2\omega}_{mp}(\mathcal{G}^{ac}_{mp} - i\Omega^{ac}_{mp}/2)(\partial F_{mp}/\partial k_b)$	Ω, $\mathcal{G}$	Ω	$\mathcal{G}$	Fermi surface
HOP	$\mathcal{I}^{\mathrm{HOP}}_{abc} = \sum_{pm} \omega_{mp} g^{2\omega}_{mp}(\mathcal{G}^{ac}_{mp} - i\Omega^{ac}_{mp}/2)(\partial g^{\omega}_{mp}/\partial k_b)F_{mp}$	Ω, $\mathcal{G}$	Ω	$\mathcal{G}$	Velocity injection along field

Here, $\mathcal{H}(\boldsymbol{k},t)=\mathcal{H}_0(\boldsymbol{k})+e\boldsymbol{r}\cdot\boldsymbol{E}(t)$ is the full Hamiltonian of the clean system, with $\mathcal{H}_0$ being the unperturbed band Hamiltonian. The last term represents the light-matter interaction in the length gauge with "$-e$" being the electronic charge. The external time dependent homogeneous electric field is given by $\boldsymbol{E}(t)=\boldsymbol{E}_0e^{-i\omega t}$, with $\boldsymbol{E}_0=\{E_0^x,E_0^y,E_0^z\}$ being the electric field strength and ω being the frequency. To simplify the analytical calculations we approximate the scattering term by ρ/τ. The relaxation time τ accounts generically for impurity and phonon scattering, as well as recombination, and is assumed to be constant.

The nonlinear dynamics of the charge carriers can be explored by expanding the density matrix perturbatively in powers of the electric field, $\rho(\boldsymbol{k},t)=\rho^{(0)}(\boldsymbol{k},t)+\rho^{(1)}(\boldsymbol{k},t)+\rho^{(2)}(\boldsymbol{k},t)+\cdots$, where $\rho^{(N)}(\boldsymbol{k},t)\propto(E_0^b)^N$. Expressing the density matrix in terms of the eigenstates of the unperturbed Hamiltonian, $\mathcal{H}_0|u_{\boldsymbol{k}}^p\rangle=\varepsilon_{p,\boldsymbol{k}}|u_{\boldsymbol{k}}^p\rangle$, the kinetic equation for the Nth order term in the density matrix, $\rho^{(N)}(\boldsymbol{k},t)\equiv\rho^{(N)}$, is given by

$$\frac{\partial\rho_{mp}^{(N)}}{\partial t}+\frac{i}{\hbar}[\mathcal{H}_0,\rho^{(N)}]_{mp}+\frac{\rho_{mp}^{(N)}}{\tau}=\frac{e\boldsymbol{E}(t)}{\hbar}\cdot[D_{\boldsymbol{k}}\rho^{(N-1)}]_{mp}. \quad (2)$$

Here, we define the covariant derivative as $[D_{\boldsymbol{k}}\rho]_{mp}=\partial_{\boldsymbol{k}}\rho_{mp}-i[\mathcal{R}_{\boldsymbol{k}},\rho]_{mp}$, where $\mathcal{R}_{mp}(\boldsymbol{k})=i\langle u_{\boldsymbol{k}}^m|\partial_{\boldsymbol{k}}u_{\boldsymbol{k}}^p\rangle$ is the momentum space band resolved Berry connection.

Up to linear order in the external field strength, the solution of Eq. (2) yields $\rho_{mp}^{(1)}=\sum_c\tilde{\rho}_{mp}^{(1,c)}E_0^ce^{-i\omega t}$, where

$$\tilde{\rho}_{mp}^{(1,c)}=\frac{e}{\hbar}g_{mp}^{\omega}[\partial_c\rho_{mp}^{(0)}\delta_{mp}+i\mathcal{R}_{mp}^cF_{mp}]. \quad (3)$$

Here, we have defined $F_{mp}\equiv f_m^{(0)}-f_p^{(0)}$ to be the difference between the occupation in bands p and m in equilibrium. The occupation of the bands is given by $f_m^{(0)}\equiv\rho_{mm}^{(0)}=[1+e^{\beta(\varepsilon_{m,\boldsymbol{k}}-\mu)}]^{-1}$ the Fermi-Dirac distribution function, where $\beta=1/(k_BT)$, k_B is the Boltzmann constant, T is the absolute temperature, and μ is the chemical potential. The function $g_{mp}^{\omega}\equiv[1/\tau-i(\omega-\omega_{mp})]^{-1}$ with $\hbar\omega_{mp}=(\varepsilon_{m,\boldsymbol{k}}-\varepsilon_{p,\boldsymbol{k}})$ is related to the joint density of states broadened by disorder, and $g_0^{\omega}=[1/\tau-i\omega]^{-1}$. The details of the calculations are given in Sec. S1 of Supplemental Material (SM) [82]. In Eq. (3), the first term captures the intraband contributions ($\rho_{mp}^{(0)}=0$ for $m\neq p$) which is finite only in the presence of a finite Fermi surface (e.g., doped semimetals and metals). The second term in Eq. (3) captures interband transitions as $F_{mp}=0$ for $m=p$.

Using the first order solution of the density matrix $\rho_{mp}^{(1)}$, the second-order correction can be calculated to be $\rho_{mp}^{(2)}=\sum_{bc}\tilde{\rho}_{mp}^{(2,bc)}E_0^bE_0^ce^{-i2\omega t}$. Here,

$$\tilde{\rho}_{mp}^{(2,bc)}=\frac{e^2g_{mp}^{2\omega}}{\hbar^2}\left[\partial_b\tilde{\rho}_{mp}^{(1,c)}-i\sum_n\left(\mathcal{R}_b^{mn}\tilde{\rho}_{np}^{(1,c)}-\mathcal{R}_b^{np}\tilde{\rho}_{mn}^{(1,c)}\right)\right], \quad (4)$$

with the second term involving a sum over all the bands. We highlight that even the intraband or diagonal terms ($m=p$) in $\rho_{mp}^{(2)}$ have contributions arising from the interband terms in $\rho_{mp}^{(1)}$ (see Sec. S1 of SM [82]).

The time dependent current is calculated from the definition, $\boldsymbol{j}(t)=-e\mathrm{Tr}[\hat{\boldsymbol{v}}\rho(t)]$. In the eigenbasis of $\mathcal{H}_0$, the velocity operator $\hat{v}^a$ can be expressed as $v_{pm}^a(\boldsymbol{k})=\hbar^{-1}(\delta_{pm}\partial_{k_a}\varepsilon_{m,\boldsymbol{k}}+i\mathcal{R}_{pm}^a\hbar\omega_{pm})$. It includes the intraband term in the form of the band velocity, and the interband term dependent on the band resolved Berry connection [84–86]. The current can also be expressed as a power series of the electric field strength, $\boldsymbol{j}(t)=\sum_N\boldsymbol{j}^{(N)}$ with $j^{(N)}\propto(E_0^b)^N$. The SH component of the current is given by the 2ω component of $j_a^{(2)}(t)$.

Explicitly calculating the SH current for a d dimensional system, we obtain

$$j_a^{(2)}(t)=-\frac{e^3}{\hbar^2}e^{-i2\omega t}\sum_{bc}E_0^bE_0^c\int_{\mathrm{BZ}}\frac{d^dk}{(2\pi)^d}\mathcal{I}_{abc}(\boldsymbol{k},\omega), \quad (5)$$

where, $\mathcal{I}_{abc}=\mathcal{I}_{abc}^{\mathrm{D}}+\mathcal{I}_{abc}^{\mathrm{Inj}}+\mathcal{I}_{abc}^{\mathrm{Sh}}+\mathcal{I}_{abc}^{\mathrm{An}}+\mathcal{I}_{abc}^{\mathrm{DR}}+\mathcal{I}_{abc}^{\mathrm{HOP}}$, and BZ denotes the Brillouin zone. Here, based on the corresponding dc counterparts [21], we have denoted the different SH contributions to the integrand as follows: Drude ($\mathcal{I}_{abc}^{\mathrm{D}}$), injection ($\mathcal{I}_{abc}^{\mathrm{Inj}}$), shift ($\mathcal{I}_{abc}^{\mathrm{Sh}}$), and anomalous ($\mathcal{I}_{abc}^{\mathrm{An}}$). In addition to these, we find two more contributions, which we refer to as the double resonant (DR) ($\mathcal{I}_{abc}^{\mathrm{DR}}$) and higher-order pole ($\mathcal{I}_{abc}^{\mathrm{HOP}}$) contributions, explained below. Both depend on the scattering time τ. Remarkably, their contributions to the current are always opposite in sign. Below, we explicitly show that the DR and HOP contributions are at least as large as the other contributions. The functional forms of all the contributions in the SH (photogalvanic) current are tabulated in Table I (Table S1 of SM [82]).

The DR current is a Fermi surface phenomenon, which shows resonant features for $\hbar\omega=\mu$ and $\hbar\omega=2\mu$ in a particle-hole symmetric system. The double resonance stems from the product of the joint density of states ($g_{mp}^{\omega}g_{mp}^{2\omega}$), reflecting the interplay of one-photon and two-photon absorption processes. The g_{mp}^{ω} factor denotes the single photon process contributing in the first order correction to the density matrix and it gives a peak at $\hbar\omega=2\mu$, in systems with particle-hole symmetry. The factor of $g_{mp}^{2\omega}$ is associated with two-photon absorption where the photon frequencies are additive, and this leads to a peak at $2\hbar\omega=2\mu$. The HOP current, on the other hand, is a Fermi sea phenomenon, its name originating from the

second-order poles in $\partial_b g^{\omega}_{mp}$. In addition to the second-order pole, the $\partial_b g^{\omega}_{mp}$ term also gives rise to velocity injection along the direction of the applied field, making the HOP contribution similar in spirit to the injection current. Among the three Fermi sea contributions, the injection current depends on the velocity difference between the two bands along the direction of current. The shift current is determined by the shift vector representing the positional shift of the carriers in real space, and the HOP current depends on the velocity difference parallel to $\boldsymbol{E}$.

Experimentally, the SH signal arising from the Fermi surface and Fermi sea contributions can be distinguished by tuning the Fermi level, particularly in 2D materials with small band gap. In $\mathcal{T}$-symmetric system, if the Fermi level lies within the band gap then only the Fermi sea terms such as the HOP and Sh contribute to the SH signal. These in turn, can be distinguished by measuring the longitudinal and Hall components, separately. The HOP term is present only in the Hall component since it originates from the band resolved Berry curvature, while the Sh term appears in both the conductivities. In $\mathcal{PT}$-symmetric system the HOP, Sh, and Inj terms can be segregated by exploiting their scattering time dependence. In the scenario, when the Fermi level lies inside the band, the total SH response near the Fermi level is mainly dictated by the dominant resonant peaks, which are dominated by the An and DR contributions. Here, the DR contribution is associated with two resonant peaks while the An contribution has a single peak.

The quantum kinetic approach can be combined with the electronic band structure obtained from *ab initio* calculation, tight-binding models, or effective low energy $\boldsymbol{k}\cdot\boldsymbol{p}$ Hamiltonian. This includes confined systems [87], magnetic materials, as well as systems with spin-orbit coupling [88]. As an example of a $\mathcal{T}$-symmetric system, we consider a two band model of monolayer WTe_2 [11,12],

$$\mathcal{H}_0(\boldsymbol{k}) = Ak^2\mathbb{1} + (Bk^2+\delta)\sigma_z + v_y k_y \sigma_y + \Delta\sigma_x. \quad (6)$$

Here, A gives tilt to the dispersion, v_y is the velocity component which gives rise to an anisotropic dispersion, and Δ controls the band gap. The $\mathcal{H}_0$ in Eq. (6) has a mirror symmetry M_x, which enforces $\mathcal{H}_0(k_x,k_y) = \mathcal{H}_0(-k_x,k_y)$. The energy dispersion for this model is given by $\varepsilon(\boldsymbol{k}) = Ak^2 \pm \sqrt{(Bk^2+\delta)^2 + k_y^2 v_y^2 + \Delta^2}$. The corresponding band structure is shown in Fig. 1(a) with the corresponding geometric quantities, the Berry curvature, and the metric connection, displayed in Fig. 1(b). Owing to the combination of mirror symmetry and $\mathcal{T}$ symmetry in Eq. (6), we have $\Omega^{xy}_{mp}(k_x,k_y) = \Omega^{xy}_{mp}(k_x,-k_y)$. This makes the BZ integrand for the SH components, $\mathcal{I}^{\mathrm{An/DR/HOP}}_{xyy}$ an odd function of k_y, and consequently $\sigma^{\mathrm{An/DR/HOP}}_{xyy} = 0$. However, the SH conductivity components $\sigma^{\mathrm{An/DR/HOP}}_{yxx}$ is finite and these generate a Hall current $j_y^{(2)} = \sigma_{yxx}E_x^2$. The real and imaginary parts of the different terms in the SH conductivity σ_{yxx} are shown in Figs. 1(c) and 1(d). The double resonant peak of $\sigma^{\mathrm{DR}}_{yxx}$ can be clearly seen in Fig. 1(c), along with the significant $\sigma^{\mathrm{HOP}}_{yxx}$ contribution. The numerical value for the conductivities in our calculations are comparable to the values recently reported for MoS_2 [89].

In contrast to $\mathcal{T}$-symmetric systems, in $\mathcal{PT}$-symmetric systems the SH generation (i) can have a finite Drude and injection contributions, (ii) have quantum geometry induced contributions which are determined solely by $\mathcal{G}$ and Γ, and (iii) the $\mathcal{G}$ induced contributions can have diagonal components of the form σ_{aaa}. An example of a $\mathcal{PT}$-symmetric material is CuMnAs, where the $\mathcal{P}$ and $\mathcal{T}$ symmetries are individually not preserved [21]. These systems generally show an antiferromagnetic ordering on the two distinct sublattice sites along with a locally broken inversion symmetry at the sublattice level (denoted below by A and B). This also gives rise to a sublattice dependent spin-orbit coupling. The corresponding Hamiltonian is given by [21,90]

$$\mathcal{H}_0(\boldsymbol{k}) = \begin{pmatrix} \epsilon_0(\boldsymbol{k}) + \boldsymbol{h}_A(\boldsymbol{k})\cdot\boldsymbol{\sigma} & V_{AB}(\boldsymbol{k}) \\ V_{AB}(\boldsymbol{k}) & \epsilon_0(\boldsymbol{k}) + \boldsymbol{h}_B(\boldsymbol{k})\cdot\boldsymbol{\sigma} \end{pmatrix}. \quad (7)$$

Here, we have defined $\epsilon_0(\boldsymbol{k}) = -t(\cos k_x + \cos k_y)$ and $V_{AB}(\boldsymbol{k}) = -2\tilde{t}\cos(k_x/2)\cos(k_y/2)$. The hopping between orbitals of the same sublattice is quantified by t, while $\tilde{t}$ denotes hopping between orbitals on different sublattices. The sublattice dependent spin-orbit coupling and the magnetization field is included in $\boldsymbol{h}_B(\boldsymbol{k}) = -\boldsymbol{h}_A(\boldsymbol{k})$, where $\boldsymbol{h}_A(\boldsymbol{k}) = \{h^x_{AF} - \alpha_R \sin k_y + \alpha_D \sin k_y, h^y_{AF} + \alpha_R \sin k_x + \alpha_D \sin k_x, h^z_{AF}\}$. The energy eigenvalues are $\varepsilon(\boldsymbol{k}) = \epsilon_0 \pm \sqrt{V_{AB}^2 + h_{Ax}^2 + h_{Ay}^2 + h_{Az}^2}$. Finite ϵ_0 breaks the particle-hole symmetry and since $h_{Ax}(-k_x,-k_y) \neq h_{Ax}(k_x,k_y)$, we have $\varepsilon(-\boldsymbol{k}) \neq \varepsilon(\boldsymbol{k})$.

The dispersion in the vicinity of one of the two band edges is shown in Fig. 2(a), along with the quantum metric (top) and the metric connection (bottom) in Fig. 2(b). We find four components of the SH conductivity to be nonzero, σ_{xxy}, σ_{xyx}, σ_{yxx} and σ_{yyy} with finite contributions from all the terms in Table I. The real and imaginary parts of σ_{yxx} are shown in Figs. 2(c) and 2(d). We find a finite contribution from the injection current (orange curve) which was absent in Fig. 1. Finite contributions from the DR and the HOP terms, comparable to the other contributions, can also be clearly seen. The resonant DR peaks deviate from $\omega = \mu$ and $\omega = 2\mu$, due to the absence of particle-hole symmetry in $\mathcal{PT}$-symmetric systems.

The quantum kinetic formulation enables us to construct a systematic quantum geometric classification of the SH response, shown in Table I. Apart from the Drude current, which depends only on the band velocity, all the other

components of the current in Table I depend on the quantum geometric properties of the electron wave function. Except for the shift current, four of these originate from the geometric quantity referred to as the quantum geometric tensor $\mathcal{Q}^{bc}_{mp} = \mathcal{R}^{b}_{pm}\mathcal{R}^{c}_{mp} = \mathcal{G}^{bc}_{mp} - (i/2)\Omega^{bc}_{mp}$ [13,91–93]. Here, the band resolved Berry curvature is antisymmetric under the exchange of spatial coordinates, $\Omega^{bc}_{mp} = -\Omega^{cb}_{mp}$, while the quantum metric is symmetric, $\mathcal{G}^{bc}_{mp} = \mathcal{G}^{cb}_{mp}$. Note that in the injection current the Cartesian indices of Ω and $\mathcal{G}$ are determined by the electric field direction. However, in the other SH components, one of the indices of Ω and $\mathcal{G}$ is determined by the direction of the current. The anomalous part of the SH current is related to the Berry curvature and quantum metric. It is easily checked that the photogalvanic counterpart ($2\omega \to 0$) of the anomalous current can be expressed as a function of the Berry curvature dipole [15]. For the shift current one can define a third rank tensor, the quantum geometric connection $\mathcal{C}^{abc}_{mp} = \mathcal{R}^{a}_{pm}\mathcal{D}^{b}_{mp}\mathcal{R}^{c}_{mp}$ with $\mathcal{D}^{b}_{mp} = \partial_b - i(\mathcal{R}^{b}_{mm} - \mathcal{R}^{b}_{pp})$, which is symmetric under the interchange of the last two spatial indices. It is decomposed into real and imaginary parts $\mathcal{C}^{abc}_{mp} = \Gamma^{abc}_{mp} - i\tilde{\Gamma}^{abc}_{mp}$ [35]. The symmetry properties of the different contributions, in $\mathcal{T}$-symmetric, and in $\mathcal{PT}$-symmetric systems are summarized in Table I and discussed in detail in SM [82].

To conclude, we have generalized the theory SH generation to include Fermi surface effects in metallic systems and the effect of disorder. We have shown that SH can act as a probe of the Berry curvature, quantum metric, and quantum geometric connection. Specifically, the SH can probe the quantum metric in $\mathcal{PT}$-symmetric systems. Our calculations have unveiled two new SH phenomena, double resonant and higher-order pole. We have provided an exhaustive quantum geometric classification of the SH and photogalvanic currents, paving the way for a full quantum geometric description of nonlinear optics.

A. A. acknowledges the Science and Engineering Research Board for Project No. MTR/2019/001520, and the Department of Science and Technology for Project No. DST/NM/TUE/QM-6/2019(G)-IIT Kanpur, of the Government of India for financial support.

*pankaj.b@srmap.edu.in
†kamaldas@iitk.ac.in
‡d.culcer@unsw.edu.au
§amitag@iitk.ac.in
‖These authors contributed equally to this work.

[1] Anyuan Gao *et al.*, Layer Hall effect in a 2D topological axion antiferromagnet, Nature (London) **595**, 521 (2021).
[2] Shen Lai, Huiying Liu, Zhaowei Zhang, Jianzhou Zhao, Xiaolong Feng, Naizhou Wang, Chaolong Tang, Yuanda Liu, K. S. Novoselov, Shengyuan A. Yang, and Wei-bo Gao, Third-order nonlinear Hall effect induced by the Berry-connection polarizability tensor, Nat. Nanotechnol. **16**, 869 (2021).
[3] Ganesh Sundaram and Qian Niu, Wave packet dynamics in slowly perturbed crystals: Gradient corrections and Berry-phase effects, Phys. Rev. B **59**, 14915 (1999).
[4] Di Xiao, Ming-Che Chang, and Qian Niu, Berry phase effects on electronic properties, Rev. Mod. Phys. **82**, 1959 (2010).
[5] Naoto Nagaosa, Jairo Sinova, Shigeki Onoda, A. H. MacDonald, and N. P. Ong, Anomalous Hall effect, Rev. Mod. Phys. **82**, 1539 (2010).
[6] Dam Thanh Son and Naoki Yamamoto, Berry Curvature, Triangle Anomalies, and the Chiral Magnetic Effect in Fermi Liquids, Phys. Rev. Lett. **109**, 181602 (2012).
[7] D. T. Son and B. Z. Spivak, Chiral anomaly and classical negative magnetoresistance of Weyl metals, Phys. Rev. B **88**, 104412 (2013).
[8] Kamal Das and Amit Agarwal, Thermal and gravitational chiral anomaly induced magneto-transport in Weyl semimetals, Phys. Rev. Res. **2**, 013088 (2020).
[9] Yang Gao, Shengyuan A. Yang, and Qian Niu, Field Induced Positional Shift of Bloch Electrons and its Dynamical Implications, Phys. Rev. Lett. **112**, 166601 (2014).
[10] Yang Gao, Semiclassical dynamics and nonlinear charge current, Front. Phys. **14**, 33404 (2019).
[11] Michał Papaj and Liang Fu, Magnus Hall Effect, Phys. Rev. Lett. **123**, 216802 (2019).
[12] Debottam Mandal, Kamal Das, and Amit Agarwal, Magnus Nernst and thermal Hall effect, Phys. Rev. B **102**, 205414 (2020).
[13] Hai-Tao Ding, Yan-Qing Zhu, Peng He, Yu-Guo Liu, Jian-Te Wang, Dan-Wei Zhang, and Shi-Liang Zhu, Extracting non-Abelian quantum metric tensor and its related Chern numbers, Phys. Rev. A **105**, 012210 (2022).
[14] J. E. Moore and J. Orenstein, Confinement-Induced Berry Phase and Helicity-Dependent Photocurrents, Phys. Rev. Lett. **105**, 026805 (2010).
[15] Inti Sodemann and Liang Fu, Quantum Nonlinear Hall Effect Induced by Berry Curvature Dipole in Time-Reversal Invariant Materials, Phys. Rev. Lett. **115**, 216806 (2015).
[16] Fernando de Juan, Adolfo G. Grushin, Takahiro Morimoto, and Joel E Moore, Quantized circular photogalvanic effect in Weyl semimetals, Nat. Commun. **8**, 15995 (2017).
[17] Yang Gao, Yinhan Zhang, and Di Xiao, Tunable Layer Circular Photogalvanic Effect in Twisted Bilayers, Phys. Rev. Lett. **124**, 077401 (2020).
[18] Tobias Holder, Daniel Kaplan, and Binghai Yan, Consequences of time-reversal-symmetry breaking in the light-matter interaction: Berry curvature, quantum metric, and diabatic motion, Phys. Rev. Res. **2**, 033100 (2020).
[19] Junyeong Ahn, Guang-Yu Guo, and Naoto Nagaosa, Low-Frequency Divergence and Quantum Geometry of the Bulk Photovoltaic Effect in Topological Semimetals, Phys. Rev. X **10**, 041041 (2020).
[20] Pankaj Bhalla, Allan H. MacDonald, and Dimitrie Culcer, Resonant Photovoltaic Effect in Doped Magnetic Semiconductors, Phys. Rev. Lett. **124**, 087402 (2020).
[21] Hikaru Watanabe and Youichi Yanase, Chiral Photocurrent in Parity-Violating Magnet and Enhanced Response in

Topological Antiferromagnet, Phys. Rev. X **11**, 011001 (2021).
[22] Hikaru Watanabe and Youichi Yanase, Photocurrent response in parity-time symmetric current-ordered states, Phys. Rev. B **104**, 024416 (2021).
[23] Jacob B. Khurgin, Current induced second harmonic generation in semiconductors, Appl. Phys. Lett. **67**, 1113 (1995).
[24] Claudio Aversa and J. E. Sipe, Nonlinear optical susceptibilities of semiconductors: Results with a length-gauge analysis, Phys. Rev. B **52**, 14636 (1995).
[25] J. E. Sipe and A. I. Shkrebtii, Second-order optical response in semiconductors, Phys. Rev. B **61**, 5337 (2000).
[26] M. M. Glazov and S. D. Ganichev, High frequency electric field induced nonlinear effects in graphene, Phys. Rep. **535**, 101 (2014).
[27] Takahiro Morimoto and Naoto Nagaosa, Topological nature of nonlinear optical effects in solids, Sci. Adv. **2**, e1501524 (2016).
[28] Takahiro Morimoto, Shudan Zhong, Joseph Orenstein, and Joel E. Moore, Semiclassical theory of nonlinear magneto-optical responses with applications to topological Dirac/Weyl semimetals, Phys. Rev. B **94**, 245121 (2016).
[29] Jacob B. Khurgin, Optically induced currents in dielectrics and semiconductors as a nonlinear optical effect, J. Opt. Soc. Am. B **33**, C1 (2016).
[30] Naoto Nagaosa and Takahiro Morimoto, Concept of quantum geometry in optoelectronic processes in solids: Application to solar cells, Adv. Mater. **29**, 1603345 (2017).
[31] Y. Tokura and N. Nagaosa, Nonreciprocal responses from non-centrosymmetric quantum materials, Nat. Commun. **9**, 3740 (2018).
[32] N. Sirica, R. I. Tobey, L. X. Zhao, G. F. Chen, B. Xu, R. Yang, B. Shen, D. A. Yarotski, P. Bowlan, S. A. Trugman, J.-X. Zhu, Y. M. Dai, A. K. Azad, N. Ni, X. G. Qiu, A. J. Taylor, and R. P. Prasankumar, Tracking Ultrafast Photocurrents in the Weyl Semimetal TaAs using THz Emission Spectroscopy, Phys. Rev. Lett. **122**, 197401 (2019).
[33] Daniel E. Parker, Takahiro Morimoto, Joseph Orenstein, and Joel E. Moore, Diagrammatic approach to nonlinear optical response with application to Weyl semimetals, Phys. Rev. B **99**, 045121 (2019).
[34] F. de Juan, Y. Zhang, T. Morimoto, Y. Sun, J. E. Moore, and A. G. Grushin, Difference frequency generation in topological semimetals, Phys. Rev. Res. **2**, 012017 (2020).
[35] Junyeong Ahn, Guang-Yu Guo, Naoto Nagaosa, and Ashvin Vishwanath, Riemannian geometry of resonant optical responses, Nat. Phys. **18**, 290 (2022).
[36] Y. Tokura and N. Nagaosa, Nonreciprocal responses from non-centrosymmetric quantum materials, Nat. Commun. **9**, 3740 (2018).
[37] Yang Gao and Di Xiao, Nonreciprocal Directional Dichroism Induced by the Quantum Metric Dipole, Phys. Rev. Lett. **122**, 227402 (2019).
[38] Lawrence D Tzuang, Kejie Fang, Paulo Nussenzveig, Shanhui Fan, and Michal Lipson, Non-reciprocal phase shift induced by an effective magnetic flux for light, Nat. Photonics **8**, 701 (2014).
[39] JunHwan Kim, Mark C Kuzyk, Kewen Han, Hailin Wang, and Gaurav Bahl, Non-reciprocal Brillouin scattering induced transparency, Nat. Phys. **11**, 275 (2015).
[40] Linbo Shao, Wenbo Mao, Smarak Maity, Neil Sinclair, Yaowen Hu, Lan Yang, and Marko Lončar, Non-reciprocal transmission of microwave acoustic waves in nonlinear parity-time symmetric resonators, National electronics review **3**, 267 (2020).
[41] X. L. Qi and S. C. Zhang, The quantum spin Hall effect and topological insulators, Phys. Today **63**, No. 1, 33 (2010).
[42] Chao-Xing Liu, Shou-Cheng Zhang, and Xiao-Liang Qi, The quantum anomalous Hall effect: Theory and experiment, Annu. Rev. Condens. Matter Phys. **7**, 301 (2016).
[43] Z. Z. Du, C. M. Wang, Hai-Zhou Lu, and X. C. Xie, Disorder-induced nonlinear Hall effect with time-reversal symmetry, Nat. Commun. **10**, 3047 (2019).
[44] S. Nandy and Inti Sodemann, Symmetry and quantum kinetics of the nonlinear Hall effect, Phys. Rev. B **100**, 195117 (2019).
[45] N. A. Sinitsyn, A. H. MacDonald, T. Jungwirth, V. K. Dugaev, and Jairo Sinova, Anomalous Hall effect in a two-dimensional Dirac band: The link between the Kubo-Streda formula and the semiclassical Boltzmann equation approach, Phys. Rev. B **75**, 045315 (2007).
[46] P. Bhalla, M.-X. Deng, R.-Q. Qang, L. Wang, and D. Culcer,, Nonlinear Ballistic Response of Quantum Spin Hall Edge States, Phys. Rev. Lett. **127**, 206801 (2021).
[47] Bruno R. Carvalho, Yuanxi Wang, Kazunori Fujisawa, Tianyi Zhang, Ethan Kahn, Ismail Bilgin, Pulickel M Ajayan, Ana M De Paula, Marcos A Pimenta, Swastik Kar *et al.*, Nonlinear dark-field imaging of one-dimensional defects in monolayer dichalcogenides, Nano Lett. **20**, 284 (2020).
[48] X. Yin, Z. Ye, D. A. Chenet, Y. Ye, K. O' Brien, J. C. Hone, and X. Zhang, Edge nonlinear optics on a MoS_2 atomic monolayer, Science **344**, 488 (2014).
[49] G. Lefkidis and W. Hübner, Phononic effects and nonlocality contributions to second harmonic generation in NiO, Phys. Rev. B **74**, 155106 (2006).
[50] Shambhu Ghimire, Anthony D. DiChiara, Emily Sistrunk, Pierre Agostini, Louis F. DiMauro, and David A. Reis, Observation of high-order harmonic generation in a bulk crystal, Nat. Phys. **7**, 138 (2011).
[51] J. E. Sipe and Ed Ghahramani, Nonlinear optical response of semiconductors in the independent-particle approximation, Phys. Rev. B **48**, 11705 (1993).
[52] D. J. Passos, G. B. Ventura, J. M. Viana Parente Lopes, J. M. B. Lopes dos Santos, and N. M. R. Peres, Nonlinear optical responses of crystalline systems: Results from a velocity gauge analysis, Phys. Rev. B **97**, 235446 (2018).
[53] Xu Yang, Kenneth Burch, and Ying Ran, Divergent bulk photovoltaic effect in Weyl semimetals, arXiv:1712.09363.
[54] Zhi Li, Ya-Qin Jin, Takami Tohyama, Toshiaki Iitaka, Jiu-Xing Zhang, and Haibin Su, Second harmonic generation in the Weyl semimetal TaAs from a quantum kinetic equation, Phys. Rev. B **97**, 085201 (2018).

[55] Kazuaki Takasan, Takahiro Morimoto, Joseph Orenstein, and Joel E. Moore, Current-induced second harmonic generation in inversion-symmetric Dirac and Weyl semimetals, Phys. Rev. B **104**, L161202 (2021).

[56] P. Bhalla and H. Rostami, Second harmonic helicity and Faraday rotation in gated single-layer $1T' - WTe_2$, Phys. Rev. B **105**, 2351232 (2022).

[57] M. Lewenstein, Ph. Balcou, M. Yu. Ivanov, Anne L'Huillier, and P. B. Corkum, Theory of high-harmonic generation by low-frequency laser fields, Phys. Rev. A **49**, 2117 (1994).

[58] Markus Lysne, Yuta Murakami, Michael Schüler, and Philipp Werner, High-harmonic generation in spin-orbit coupled systems, Phys. Rev. B **102**, 081121(R) (2020).

[59] Dasol Kim, Dongbin Shin, Alexandra S. Landsman, Dong Eon Kim, and Alexis Chacn, Theory for all-optical responses in topological materials: The velocity gauge picture, arXiv:2105.12294.

[60] F. de Juan, Y. Zhang, T. Morimoto, Y. Sun, J. E. Moore, and A. G. Grushin, Difference frequency generation in topological semimetals, Phys. Rev. Res. **2**, 012017 (2020).

[61] Pavan Hosur, Circular photogalvanic effect on topological insulator surfaces: Berry-curvature-dependent response, Phys. Rev. B **83**, 035309 (2011).

[62] S. A. Mikhailov, Theory of the giant plasmon-enhanced second-harmonic generation in graphene and semiconductor two-dimensional electron systems, Phys. Rev. B **84**, 045432 (2011).

[63] Yang Zhang, Yan Sun, and Binghai Yan, Berry curvature dipole in Weyl semimetal materials: An *ab initio* study, Phys. Rev. B **97**, 041101(R) (2018).

[64] Habib Rostami and Marco Polini, Nonlinear anomalous photocurrents in Weyl semimetals, Phys. Rev. B **97**, 195151 (2018).

[65] Jhih-Shih You, Shiang Fang, Su-Yang Xu, Efthimios Kaxiras, and Tony Low, Berry curvature dipole current in the transition metal dichalcogenides family, Phys. Rev. B **98**, 121109(R) (2018).

[66] L. E. Golub and E. L. Ivchenko, Circular and magneto-induced photocurrents in Weyl semimetals, Phys. Rev. B **98**, 075305 (2018).

[67] Junchao Ma, Qiangqiang Gu, Yinan Liu, Jiawei Lai, Peng Yu, Xiao Zhuo, Zheng Liu, Jian-Hao Chen, Ji Feng, and Dong Sun, Nonlinear photoresponse of Type-II Weyl semimetals, Nat. Mater. **18**, 476 (2019).

[68] Y. Okamura, S. Minami, Y. Kato, Y. Fujishiro, Y. Kaneko, J. Ikeda, J. Muramoto, R. Kaneko, K. Ueda, V. Kocsis, N. Kanazawa, Y. Taguchi, T. Koretsune, K. Fujiwara, A. Tsukazaki, R. Arita, Y. Tokura, and Y. Takahashi, Giant magneto-optical responses in magnetic Weyl semimetal $Co_3Sn_2S_2$, Nat. Commun. **11**, 4619 (2020).

[69] Naotaka Yoshikawa, Kohei Nagai, Kento Uchida, Yuhei Takaguchi, Shogo Sasaki, Yasumitsu Miyata, and Koichiro Tanaka, Interband resonant high-harmonic generation by valley polarized electron-hole pairs, Nat. Commun. **10**, 3709 (2019).

[70] Liang Z. Tan and Andrew M. Rappe, Upper limit on shift current generation in extended systems, Phys. Rev. B **100**, 085102 (2019).

[71] Jesús Iñarrea, Resonance peak shift in the photocurrent of ultrahigh-mobility two-dimensional electron systems, Phys. Rev. B **101**, 115419 (2020).

[72] Hua Wang and Xiaofeng Qian, Electrically and magnetically switchable nonlinear photocurrent in PT-symmetric magnetic topological quantum materials, npj Comput. Mater. **6**, 199 (2020).

[73] Ruixiang Fei, Wenshen Song, and Li Yang, Giant photogalvanic effect and second-harmonic generation in magnetic axion insulators, Phys. Rev. B **102**, 035440 (2020).

[74] Lingyuan Gao, Zachariah Addison, E. J. Mele, and Andrew M. Rappe, Intrinsic Fermi surface contribution to the circular photogalvanic effect, Phys. Rev. Res. **3**, L042032 (2021).

[75] Haiyang Zou, Guozhang Dai, Aurelia Chi Wang, Xiaogan Li, Steven L. Zhang, Wenbo Ding, Lei Zhang, Ying Zhang, and Zhong Lin Wang, Alternating current photovoltaic effect, Adv. Mater. **32**, 1907249 (2020).

[76] Daniel Kaplan, Tobias Holder, and Binghai Yan, Momentum shift current at terahertz frequencies in twisted bilayer graphene, Phys. Rev. Res. **4**, 013209 (2022).

[77] Yang Gao and Furu Zhang, Current-induced second harmonic generation of Dirac or Weyl semimetals in a strong magnetic field, Phys. Rev. B **103**, L041301 (2021).

[78] Yadong Wei, Weiqi Li, Yongyuan Jiang, and Jinluo Cheng, Electric field induced injection and shift currents in zigzag graphene nanoribbons, Phys. Rev. B **104**, 115402 (2021).

[79] Swati Chaudhary, Cyprian Lewandowski, and Gil Refael, Shift-current response as a probe of quantum geometry and electron-electron interactions in twisted bilayer graphene, arXiv:2107.09090.

[80] Li-kun Shi, Dong Zhang, Kai Chang, and Justin C. W. Song, Geometric Photon-Drag Effect and Nonlinear Shift Current in Centrosymmetric Crystals, Phys. Rev. Lett. **126**, 197402 (2021).

[81] Dimitrie Culcer, Akihiko Sekine, and Allan H. MacDonald, Interband coherence response to electric fields in crystals: Berry-phase contributions and disorder effects, Phys. Rev. B **96**, 035106 (2017).

[82] See Supplemental Material at http://link.aps.org/supplemental/10.1103/PhysRevLett.129.227401 for discussions of (i) quantum kinetic theory to compute the electric field induced linear and second-order corrections to the density matrix, (ii) symmetry properties of different geometric quantities involved in the SH generation, (iii) symmetry analysis of the different contributions to the SH currents, and (iv) model specific calculations for $\mathcal{T}$ symmetric, and $\mathcal{PT}$ symmetric systems.

[83] Enrico Rossi, Quantum metric and correlated states in two-dimensional systems, Curr. Opin. Solid State Mater. Sci. **25**, 100952 (2021).

[84] Frank Wilczek and A. Zee, Appearance of Gauge Structure in Simple Dynamical Systems, Phys. Rev. Lett. **52**, 2111 (1984).

[85] Dimitrie Culcer, Yugui Yao, and Qian Niu, Coherent wave packet evolution in coupled bands, Phys. Rev. B **72**, 085110 (2005).

[86] Ming-Che Chang and Qian Niu, Berry curvature, orbital moment, and effective quantum theory of electrons in electromagnetic fields, J. Phys. Condens. Matter **20**, 193202 (2008).
[87] J. E. Moore and J. Orenstein, Confinement-Induced Berry Phase and Helicity-Dependent Photocurrents, Phys. Rev. Lett. **105**, 026805 (2010).
[88] James H. Cullen, Pankaj Bhalla, E. Marcellina, A. R. Hamilton, and Dimitrie Culcer, Generating a Topological Anomalous Hall Effect in a Nonmagnetic Conductor: An In-Plane Magnetic Field as a Direct Probe of the Berry Curvature, Phys. Rev. Lett. **126**, 256601 (2021).
[89] Yilei Li, Yi Rao, Kin Fai Mak, Yumeng You, Shuyuan Wang, Cory R. Dean, and Tony F. Heinz, Probing symmetry properties of few-layer MoS_2 and h-BN by optical second-harmonic generation, Nano Lett. **13**, 3329 (2013).
[90] L. Šmejkal, J. Železný, J. Sinova, and T. Jungwirth, Electric Control of Dirac Quasiparticles by Spin-Orbit Torque in an Antiferromagnet, Phys. Rev. Lett. **118**, 106402 (2017).
[91] J. P. Provost and G. Vallee, Riemannian structure on manifolds of quantum states, Commun. Math. Phys. **76**, 289 (1980).
[92] Yu-Quan Ma, Shu Chen, Heng Fan, and Wu-Ming Liu, Abelian and non-Abelian quantum geometric tensor, Phys. Rev. B **81**, 245129 (2010).
[93] Da-Jian Zhang, Qing-hai Wang, and Jiangbin Gong, Quantum geometric tensor in $\mathcal{PT}$-symmetric quantum mechanics, Phys. Rev. A **99**, 042104 (2019).